Integrated dielectrophoretic and surface plasmonic platform for million-fold improvement in the detection of fluorescent events

Logeeshan Velmanickam,[1] Michael Fondakowski,[2] Ivan T. Lima, Jr.,[1] and Dharmakeerthi Nawarathna[1]
[1]*Department of Electrical and Computer Engineering, North Dakota State University, Fargo, North Dakota 58102-6050, USA*
[2]*Department of Mechanical Engineering, North Dakota State University, Fargo, North Dakota 58102-6050, USA*

(Received 28 April 2017; accepted 11 August 2017; published online 22 August 2017)

We present an integrated dielectrophoretic (DEP) and surface plasmonic technique to quantify ∼1 pM of fluorescent molecules in low conductivity buffers. We have established a DEP force on target molecules to bring those molecules and place them on the nanometallic structures (hotspots) for quantification through surface plasmonic effects. Our results show that the DEP is capable of placing the fluorescent molecules on the hotspots, which are depicted as a significant reduction in the fluorescence lifetime of those molecules. To efficiently integrate the DEP and plasmonic effects, we have designed and utilized pearl-shaped interdigitated electrodes (PIDEs) in experiments. These electrodes generate 2–3 times higher DEP force than traditional interdigitated electrodes. Therefore, high-throughput assays can be developed. The nanometallic structures were strategically fabricated in the periphery of PIDEs for smooth integration of DEP and plasmonic detection. With the introduction of DEP, about 10^6-fold improvement was achieved over existing plasmonic-based detection. Therefore, this simple addition to the existing surface plasmonic-based detection will enable the disease related protein detection. *Published by AIP Publishing.* [http://dx.doi.org/10.1063/1.5000008]

INTRODUCTION

Quantification of biomarker molecules such as proteins, DNA, and RNA in biological samples (e.g., blood, saliva, and serum) is routinely performed to assess various stages of diseases and to develop therapeutic strategies for disease elimination or control (Jolley *et al.*, 1984 and Lisi *et al.*, 1982). Among the promising methods to quantify these biomarker molecules, fluorescence-based optical sensing techniques involve fluorescently labeling and measuring the fluorescence intensity of the target biomarkers in the sample. The fluorescence intensity is then converted into molarity and the number of target molecules (Epstein and Walt, 2003). The detection limit (or limit of detection) is an important factor in sensing because it indicates the smallest amount of detectable molecules. The limit of fluorescence detection is not sufficient to detect many disease-related biomarkers, especially in the early stages of disease development (Patterson *et al.*, 1997). To address this issue, interactions of metal surfaces, particles, and colloids with fluorophore molecules have been utilized in assays. These metallic components increase the electric field (felt by the fluorophore) and subsequently decrease the radiative decay rate of the fluorophore (Lakowicz, 2001). The radiative decay rate is the spontaneous rate at which a fluorophore emits photons (Lakowicz, 2001). These effects cause a significant increase in the quantum yield and decrease in the fluorescence lifetime (Lakowicz, 2001). As a direct result, the fluorescence intensity of the fluorophore significantly increases, and the fluorophore can easily be recognized from the background white noise (Lakowicz, 2001). Therefore, the detection limit of the fluorescence-based assays can be significantly improved. Studies using

silver or gold colloidal metal films and placing fluorophore molecules near those metals have reported producing undesirable chemical reactions between the fluorophore and metals such as metal etching by halide ions (Geddes and Lakowicz, 2002). Therefore, additional studies were performed with modified metal colloidal films using about 10-nm glass films, and these studies reported an approximate 20-fold enhancement of fluorescence (Geddes and Lakowicz, 2002).

Additionally, nano-fabricated metallic nano-structures have been used in experiments to further improve the fluorescence enhancement of fluorescence-based assays (Fu *et al.*, 2010 and Lakowicz, 2001). Fabrication of metallic nano-structures is typically performed using an E-beam lithography tool (Mendes *et al.*, 2004). Unfortunately, production of metallic nano-structures using an E-beam lithography tool is a complicated process that is expensive and time-consuming and can produce only a small amount of nano-structures that can handle only small sample volumes. Thus, nano-fabricated metallic nanostructures with E-beam lithography are not feasible in a real diagnosis assay. To address this issue, studies have focused on producing metallic nano-structures using non-conventional methods (Fu *et al.*, 2010 and Barik *et al.*, 2014). These nano-structures are easy to manufacture, cost effective, and sufficient for handling large sample volumes. With these structures, studies have focused on improving the detection limits and sensitivity of fluorescence-based assays, particularly using the fluorophore and metal interactions, which are also called as surface plasmonic effects (Fu *et al.*, 2010 and Barik *et al.*, 2014). In these methods, the interaction of metallic nanostructures and fluorescently labeled biomarkers near metal and dielectric interfaces was utilized to quantify biomarkers as they increase fluorescence intensity (Fu *et al.*, 2010; White *et al.*, 2012; and Dutta Choudhury *et al.*, 2012). For example, Fu *et al.* demonstrated an increase of up to 4000-fold in the fluorescence emission (Fu *et al.*, 2010).

To drastically improve the detection limit of all these plasmonic-based sensing techniques, fluorescently labeled biomarkers would need to be placed within about 100 nm from metallic nanostructures (hotspots) (Fu *et al.*, 2010; Geddes and Lakowicz, 2002; and Lakowicz, 2001). Because of this limitation, detection is limited to the molecules that are about <100 nm from hotspots. To address this issue, we have used dielectrophoretic force (DEP) to place the biomarkers on hotspots and studied the fluorescence intensity and lifetime. DEP is a direct result of dielectrophoresis, a process in which biomolecules experience a force, resulting in movement to the area that has the highest or lowest electric field gradient $\nabla(|E|^2)$ (Nawarathna *et al.*, 2009). Theoretical studies have shown that metallic nanostructures produce a greater fluorescence enhancement compared with the colloidal metal films, and thus, we selected metallic nanostructures for our study (Geddes and Lakowicz, 2002).

Studies have used DEP to manipulate DNA, messenger ribonucleic acid (mRNA), micro ribonucleic acid (miRNA), and protein molecules (Pommer *et al.*, 2008; Nawarathna *et al.*, 2009; Cheng *et al.*, 2010; Zheng *et al.*, 2004; Nakano and Ros, 2013; and Liao *et al.*, 2012). Additionally, studies have utilized integrated approaches that combine DEP with other methods to detect biomolecules (Cheng *et al.*, 2010 and Sanghavi *et al.*, 2015). In this study, we used fluorescently labeled Avidin (protein) molecules. Detection of protein is specifically important in diagnosis, but most protein detection applications currently rely on traditional methods such as spectrometry and antibody-dependent methods. However, there are several sensitive methods available for detection of nucleic acids (DNA, mRNA, and miRNA), such as real-time polymerase chain reaction, micro-array techniques, and gel electrophoresis (Wolcott, 1992). These methods are commonly used, and detection limits down to a few molecules are possible using these methods. In this regard, studies have reported detecting up to fM levels of nucleic acids (Cheng *et al.*, 2010).

Dielectric properties of nucleic acids were investigated by a number of research groups, and it was reported that nucleic acids have semiconducting-like properties (Zheng *et al.*, 2004 and Clarke *et al.*, 2005). In addition, frequency dependent polarization mechanisms are well understood for nucleic acid molecules (Cuervo *et al.*, 2014 and Pethig, 2010). Therefore, designing and implementation of assays that involve DEP forces are doable. In comparison, studies have reported that dielectric properties of proteins are more diverse than nucleic acids and dependent on the number of parameters such as buffer conditions, molarity, and size of the proteins (Zheng *et al.*, 2004). Therefore, development of sensing assays that use DEP is

challenging. Studies that are focused only on using plasmonic effects to detect proteins have reported the detection limit of 1 μM (Kim *et al.*, 2009 and Rusling *et al.*, 2010). Therefore, in this study, our starting molarity of Avidin molecules that we have used in experiments was 1 μM. Since the DEP force on protein molecules is significantly weaker than nucleic acids, we have developed a new electrode array that produces large electric field gradients. This high electric field gradient produces large DEP force on protein molecules. Since we integrate DEP force and plasmonic effects of fluorescently labeled protein molecules, there must be a simple and scalable electrode design and micro-fabrication method that allows the production of integrated metal structures with hotspots. In this study, we have developed, tested, and manufactured Pearl-shaped Interdigitated Electrodes (PIDEs) for integrated DEP and plasmonic experiments. We will present a detailed description about each important component of our method, experiments, and results below.

METHODS

Mathematically, DEP force acting on biomarker molecules is represented as

$$F_{DEP} = \frac{1}{2}\alpha \nabla\left(|E|^2\right), \tag{1}$$

where α is the polarizability of the biomarker, ∇ is the gradient operator, and E is the root-mean square (r.m.s) of the electric field (Nawarathna *et al.*, 2009). For a spherical particle

$$\alpha = 4\pi\varepsilon_m r^3 \boldsymbol{Re}\left\{f_{CM}(\omega)\right\}, \tag{2}$$

where r is the radius of the particle, ε_m is the suspending medium permittivity, ω is the frequency of the applied electric field, and $\boldsymbol{Re}\left\{f_{CM}(\omega)\right\}$ the real part of the Clausius-Mossotti factor is defined as

$$f_{CM}(\omega) = \left(\varepsilon_p^* - \varepsilon_m^*\right)/\left(\varepsilon_p^* + 2\varepsilon_m^*\right), \tag{3}$$

where ε_p^* is the complex permittivity of the particle and ε_m^* is the complex permittivity of the suspending medium (Pethig, 2010). The complex permittivity is given by $\varepsilon^* = \varepsilon - j\left(\frac{\sigma}{\omega}\right)$ with σ being the real conductivity, ε the real permittivity, and ω the frequency (Pethig, 2010). The real part of the Clausius-Mossotti factor is theoretically bounded between $-1/2$ and 1, which determines the direction and the relative strength of the DEP force. If the magnitude of $\mathrm{Re}\{f_{CM}(\omega)\}$ is negative, then the particles are repelled from the electrodes and move towards the location where there is the lowest field gradient (negative DEP). Similarly, for positive values of $\mathrm{Re}\{f_{CM}(\omega)\}$, particles are attracted to the electrode edges where there is the highest electric field gradient (positive DEP). However, for particles suspended in low conductivity buffers, at lower frequencies (<50 MHz), f_{CM} is dependent on the medium (σ_m) and particle conductivity values (σ_p) (Pethig, 2010). σ_p of the particle can be written as the sum of bulk conductivity (σ_pbulk) and surface conductance ($\mathrm{K_S}$), which can be represented as $\sigma_\mathrm{p} = \sigma_\mathrm{pbulk} + (\mathrm{K_S}/\mathrm{r})$. Furthermore, for small particles (when $r \to 0$), σ_p is dependent on the $\mathrm{K_S}$ value (Hughes *et al.*, 1999; Ermolina and Morgan, 2005; and Basuray and Chang, 2007).

Since the positive DEP force concentrates particles near the electrode edges where we have plasmonic hotspots, we have used positive DEP throughout our study. A large DEP force is always desirable because it enables the development of high-throughput assays. Large electric field gradients $\nabla(|E|^2)$ are typically required to produce a large DEP force on molecules (Li and Bashir, 2002 and Kim *et al.*, 2004). Interdigitated electrodes (IDE) have been commonly used in the DEP experiments [Pethig, 2010]. IDEs have been used in high-throughput manipulation of biological cells and molecules (Li and Bashir, 2002 and Zou *et al.*, 2007). IDEs provide a simple electrode structure that generates the extremely high electric field gradients needed for DEP-based cell/molecule manipulation. In addition to IDEs, other electrode configurations like cusp-shaped nanocolloid assemblies have been used in DEP experiments (Cheng *et al.*, 2010).

Since we use DEP and plasmonic-based detection, traditional IDEs or any other electrode configurations are not a viable solution for our experiments. Therefore, we designed and used PIDEs. Pictures of our PIDEs are shown in Figs. 1(a), 1(b), and 1(d). In comparison with traditional IDEs, PIDEs are capable of generating higher electric field gradients $\nabla(|E|^2)$ than traditional IDEs. Typically, our PIDEs are generating about two to three times higher electric field gradients than the traditional IDEs (Nawarathna *et al.*, 2009 and Gupta *et al.*, 2012).

A number of nano-scale metal structures (e.g., Bowtie nano-apertures) have been successfully used in the context of plasmonic-based fluorescence detection (Lu, 2012; Mulvihill *et al.*, 2009; and Maier and Atwater, 2005). In addition to these planar nano-scale metallic structures, studies have used nano-capillaries in plasmonic-based fluorescently labeled nucleic acid detection (Čemažar *et al.*, 2016). Since we are combining DEP and plasmonic effects in our experiments, moreover, using DEP force to place molecules on the hotspots, these plasmonic structures are not directly applicable to our experiments. Further, fabrication of those nano-scale metal structures requires sophisticated equipment (e.g., electron beam lithography) and nanofabrication facilities. Therefore, first, we have designed and fabricated a new electrode design (PIDE) that allows us to establish a large DEP force on molecules while at the same time producing hotspots for the detection of molecules using plasmonic effects.

We then fabricated PIDEs using standard microfabrication techniques. The details of the fabrication are published elsewhere (Pommer *et al.*, 2008). We produced hotspots in the periphery of the pearls of our PIDEs. The production of hotspots was achieved through careful overexposing of photoresists films to UV light during photolithography. We then developed the photoresist films, sputtered 1000 Å Au, and lifted off the photoresist film in acetone. This fabrication process produced a large number of hotspots with various shapes and sizes. A few of the shapes of the hotspots are shown in Figs. 1(e)–1(g). This was a repeatable fabrication process that we used to produce hotspots throughout this paper. Our manufacturing process did not use the E-beam lithography tool. Further, production of hotspot is a part of the traditional photolithography process. Therefore, production of a large number of hotspots needed to accommodate clinical sample volumes (typically few milliliters) is technically possible.

To gain a deep understanding on how the integration of DEP and hotspots potentially enhances the surface-plasmonic effects, we used a scanning electron microscope (SEM) to image the locations of the hotspots and an energy dispersive spectroscope (EDS) to perform an elemental analysis of the hotspots (Nawarathna *et al.*, 2013). The SEM images were used to measure the dimensions of the hotspots [see Figs. 1(d)–1(g)]. However, SEM images do not

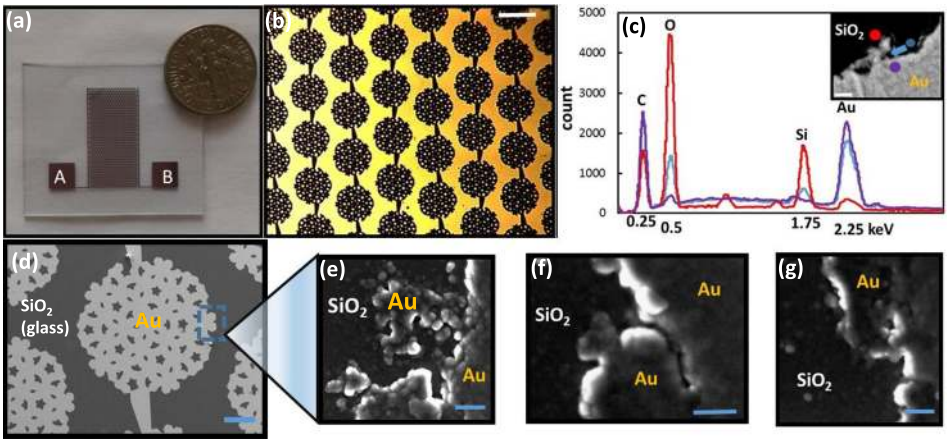

FIG. 1. Fabrication and characterization of PIDEs and hotspots for fluorescence experiments. (a) Final version of the device that we have used in experiments. External electric potential was applied at A and B. (b) Close-up view of the PIDE array showing how PIDEs are designed and fabricated (scale bar 200 μm). (c) Characterization of the hotspots using EDS. The hotspot shown in the inset was characterized using EDS, and spectra are shown in the figure. The scale bar of the inset is 100 nm. (d) Characterization of the hotspots using SEM. Low magnification view of a PIDE (scale bar: 50 μm). (e), (f), and (g) The SEM images showing hotspots of various sizes and shapes (scale bar: 200 nm).

provide detailed elemental characterization of hotspots (locations of metals and dielectrics). For example, for the SEM image shown in Fig. 1(c), we have used the EDS to find out if there is a residual photoresist films or any other metallic or non-metallic contaminations are still remaining in the hotspot (indicated by blue dots). These contaminations will be visible in the EDS spectrum. We have used the "point-and-shoot" technique in the EDS software and determined the elements present in the hotspots. A typical result of an EDS analysis of a hotspot is indicated in Fig. 1(c). Note that if the positive DEP-placed biomarker molecules on the dielectric material are between the gold electrode (violet color dot) and the gold arm (red color dot), it will be subjected to surface plasmonic effects.

To quantitatively understand the electric field gradient, $\nabla(|E|^2)$, generated by the PIDE structures, we have used the AC/DC module of commercially available COMSOL (COMSOL, Inc.) software and calculated the expected electric field gradients. In this calculation, the PIDEs were first drawn to scale using AutoCAD (Autodesk) software and then imported into the COMSOL software. We then assumed that a buffer solution ($\sigma = 0.03$ S/m and $\varepsilon_r = 80.3$) filled the space above the electrodes. We used the swept mesh technique to mesh PIDEs. This is needed to properly mesh nano- and microscale features of our electrodes. Briefly, first, we meshed x-y ($z = 0$) plane of the electrode using "Free Triangular Mesh" with the maximum element size of 90 nm and the minimum element size of 1 nm. We then swept the "Free Triangular Mesh" in the z direction with minimum and maximum mesh sizes of 5 nm and 1 nm, respectively. This procedure allowed us to successfully mesh our electrodes. Further, we also assumed that an external potential with a frequency (120 kHz) and voltage (1 Vpp) was applied to the electrodes. This is the AC potential that we have used in our DEP experiments. We chose 120 kHz because it has been reported that the positive DEP force will be maximum at 120 kHz for biomarker molecules (Nawarathna *et al.*, 2009). Finally, we calculated the electric field from which we extracted the electric field gradient in the vicinity of our PIDE structures.

In Fig. 2(a), we show the calculated electric field gradient in the x-y plane ($z = 100$ nm) of the PIDEs. There are high and low electric field gradient regions in the PIDE; blue colored regions have the lowest electric field gradient ($\sim 10^{12}$ V^2/m^3) and red colored regions have the highest electric field gradients ($\sim 3 \times 10^{15}$ V^2/m^3) (Nawarathna *et al.*, 2009). We then calculated

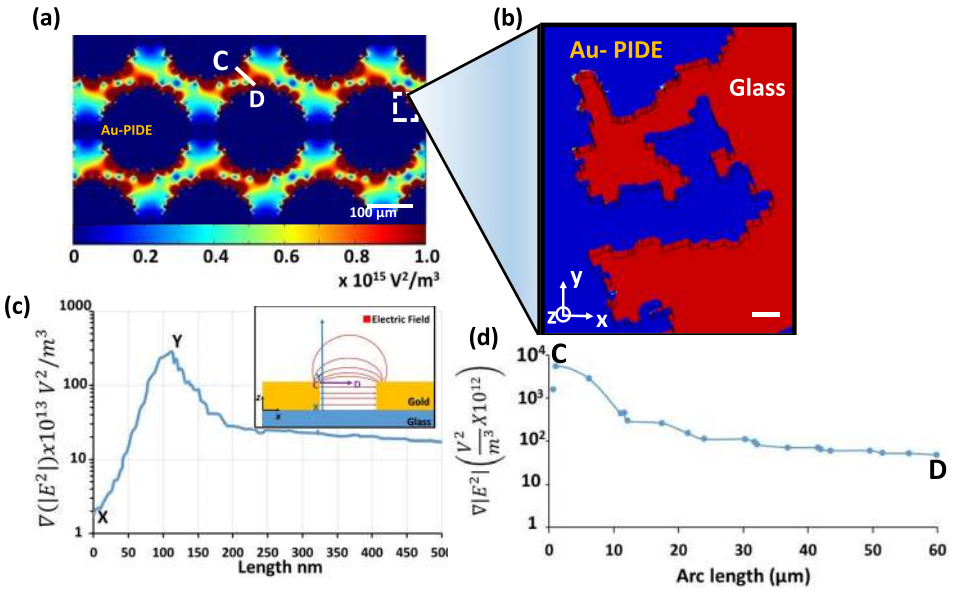

FIG. 2. Calculated electric field gradients ($\nabla(|E|^2)$) near the electrodes and hotspots. (a) Calculated electric field gradients on the PIDEs in the x-y plane ($z = 100$ nm). (b) Close-up view of the electric field gradient of hotspots in the $z = 100$ nm plane. We have used Fig. 1(e) for this calculation. The scale bar indicates 200 nm. (c) Variation of the electric field gradient in the z direction. "X" indicates the $z = 100$ nm plane and "Y" is the top plane of the hotspots. (d) Variation of the electric field gradient along the contour C-D [$z = 100$ nm, Fig. 2(a)].

the variation of the electric field gradient along the contour C-D [Fig. 2(d)]. According to this calculation, in comparison, the DEP force is only about 70–80 times smaller at 60 μm (point D) than the DEP force at point C. To further understand the DEP-assisted molecular placing in the hotspots, we calculated the energy $\left(\frac{1}{2}\,\alpha E^2\right)$ provided by the external electric field to the molecules. We then compared the electric energy with the ground state energy of the molecules (kT; k is the Boltzmann constant; T is the average temperature on the electrodes). For the DEP force to be effective, the energy provided by the external electric field must be greater than the ground state energy of the molecules. For comparison, we calculated these energies along the contour C-D, and the results are shown in Fig. 3(a). Since the energy provided by the electric field is larger than the ground state energy, it can be concluded that positive DEP will bring molecules from 50 to 60 μm away from the interface and place molecules on the hotspots for quantification through surface plasmonic effects. Since this calculation shows the variation of $\nabla(|E|^2)$ in the x-y plane (along the contour C-D), we performed another calculation to find the variation of $\nabla(|E|^2)$ in the z direction. The $\nabla(|E|^2)$ in the z direction will produce DEP force on molecules in the z-direction. In parallel, we have used the formula (above) and calculated the energy provided to the molecules by the electric field. We then compared the energy of the molecules to the ground state energy of the molecules. Our calculation shows that, at $z = 500\,\text{nm}$ ($x = y = 0$), energy provided by the electric field is about 4 times greater than the ground state of the molecules. Therefore, the electric field gradient in the z direction will produce a sufficiently large DEP force to bring molecules from the z direction and combine with DEP in the x-y to place molecules in the hotspots. Furthermore, molecules that are far away from electrodes ($z \gg 500\,\text{nm}$) will not be capable of using the DEP force to get trapped in the hotspots. One can use other forces such as electrophoretic force to bring those molecules to closer to the electrodes so that DEP force will be strong enough to place them in the hotspots. Other option will be to design the height of the channel within the DEP active area. Then, DEP force will be sufficient to trap all the molecules in the hotspots. Figure 2(b) illustrates the variation of $\nabla(|E|^2)$ in the $z = 100\,\text{nm}$ plane and Fig. 2(c) shows the variation of $\nabla(|E|^2)$ in the x-z plane. From these analyses, it can be concluded that the highest $\nabla(|E|^2)$ is generated at the top edge of the hotspots [Fig. 2(c)]. Therefore, these top edges [indicated as "Y" in Fig. 2(c)] will have a large number of molecules collected through DEP. This analysis agrees with the experimental results in the Fig. 5(a) inset, where we observed the concentrating molecules at the top edges of the hotspots.

Next, we performed another COMSOL calculation to find the expected electric field enhancement near hotspots from the plasmonic effects. This electric field enhancement is expected when we excite the fluorescent biomarker molecules using the appropriate light source. To perform the calculation, we first drew the hotspots in AutoCAD software using a SEM image of our actual hotspots [Fig. 1(e)] and imported into the COMSOL software. We then used the

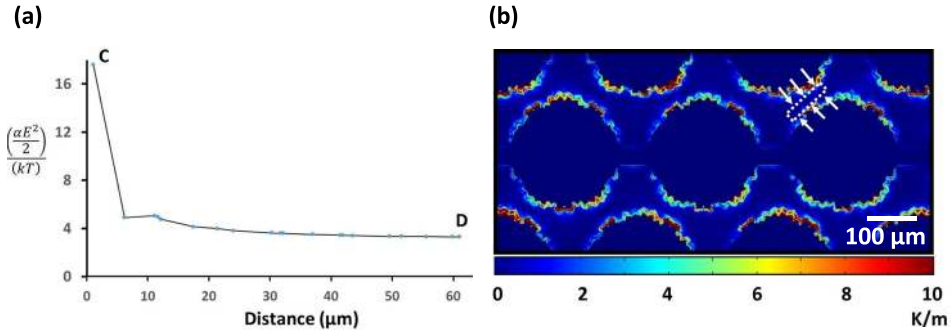

FIG. 3. Comparison of energy harvested by biomolecules from the AC electric field to ground state energy and thermophoretic effects on molecules. (a) Comparison of energy harvested from the electric field to ground state energy. Note that almost all molecules that are in the sample harvest at least four times more energy than the ground state energy. (b) Calculation of the temperature gradient near electrodes. This temperature gradient will produce thermophoretic forces on biomolecules.

wave optics module of the COMSOL software and solved the traditional wave equation. In this application, when we assume the electric field as a planar traveling wave, the wave equation transform into Eq. (4). COMSOL software solved the Eq. (4) and calculated the expected electric field distribution and electric field enhancement near hotspots

$$\nabla \times \mu^{-1}(\nabla \times E) - k_0^2\left(\varepsilon_r - \frac{j\sigma}{\omega\varepsilon_0}\right)E = 0, \tag{4}$$

where E is the electric field, μ = permittivity, k_0 = wave number, σ = electric conductivity, ϵ_r = relative dielectric constant, ϵ_0 = dielectric constant of air, and ω = angular frequency. We have also assumed that hotspots were made out of Au and a transverse electric wave with a 500 nm wavelength and 1mW power passing through the hotspots. A 500-nm wavelength was chosen because it is close to the actual excitation wavelength that we have used in experiments. Figure 4(a) indicates the electric field distribution near hotspots. As we would expect, there is a large electric field near hotspots. The published literature has been shown similar electric field distribution near metallic nanostructures (Iandolo *et al.*, 2013). For comparison, we calculated the electric field variation across the contour A-B. This will also provide good understanding of how the electric field varies across the hotspots. The contour A-B goes across a number of hotspots and Fig. 4(b) shows the electric field enhancement across A-B and the maximum electric field enhancement near our hotspots is about sixfold. Most of the published literature studies have reported about a threefold electric field enhancement (Fu *et al.*, 2010). This electric field enhancement directly contributes to the fluorescence of Avidin molecules. Studies have shown that the enhanced electric field increases the fluorescence emission of Avidin molecules through the "Lightning Rod Effect" (Geddes and Lakowicz, 2002). In addition, the plasmonic hotspots decrease the radiative decay rate of the fluorophore and therefore lifetime of the fluorophore will have a reduction (Geddes and Lakowicz, 2002). Through this characterization, we have fully understood the abilities of electrodes to generate DEP and plasmonic effects.

In this high electric field and its gradients, there can be significant Joule heating resulting in a temperature increase near the electrodes. If the temperature is too high, the molecules that are being detected will be exposed to the high temperature and loss of their functionality. To understand the Joule heating in our PIDEs, we have calculated the temperature increase $[\Delta T = (T_{actual} - T_{room})$; $T_{room} = 300\,\mathrm{K}]$ in our PIDEs using COMSOL software. Briefly, we first calculated the electrical energy supplied to the surroundings through PIDEs. We then assumed that electrical energy is converted into the thermal energy through the temperature increase. Through this calculation, we have found that a roughly 2° temperature increase (above the room temperature) will take place during the experiments, and this temperature will not cause

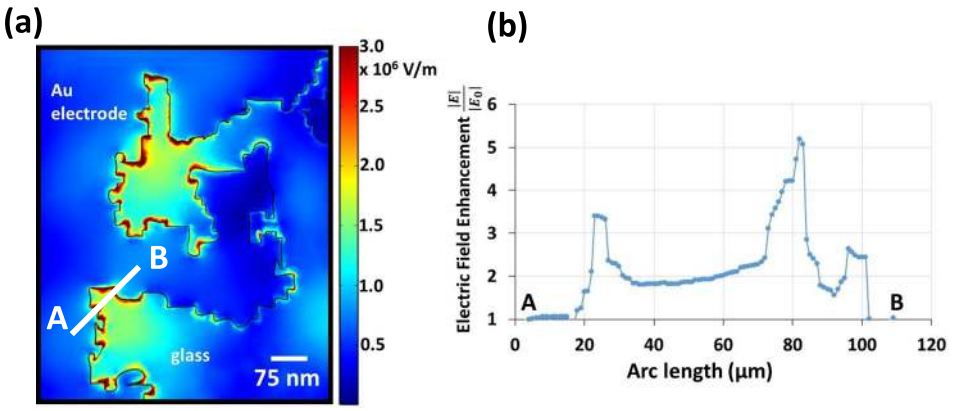

FIG. 4. Calculated electric enhancements due to the plasmonic effects. (a) We have used the SEM image of Fig. 1(e) and used the COMSOL software to calculate the expected electric fields in the sample when 1mW light was applied perpendicular to the sample. (b) Calculated electric field enhancement along the contour A-B of (a). This demonstrates the typical electric field enhancement that we expect from the hotspots. E_o is the electric field that is away from the hotspots.

any damage to the molecules. This result (temperature increase) can be deduced from the published work by others (Nakano *et al.*, 2014; Chaurey *et al.*, 2013; and Lu *et al.*, 2015). In addition, under this temperature distribution, one expects thermophoretic force (TP) on molecules through thermophoresis. The TP force on molecules causes thermodiffusion, (j), which is mathematically represented as

$$\vec{j} = -D_T c \nabla T \tag{5}$$

where D_T is the thermophoretic mobility, c is the concentration of molecules, and ∇T is the temperature gradient. According to Eq. (5), the TP will push the molecules away from the places where there are high temperature gradients. To further understand the motion of molecules through TP, we have extended our temperature calculation and determined ∇T. Figure 3(b) indicates the variation of ∇T on our sample. The thermodiffusion will push the molecules away from the electrode boundaries to the region indicated in the white box in Fig. 3(b). At the same time, DEP will attract the molecules toward the electrode boundaries [Fig. 2(a)]. If the electrodiffusion is dominant, there must be an accumulation of molecules in the area indicated by the white rectangle [Fig. 3(b)]. However, in experiments, we did not observe any accumulation of molecules in that area [Fig. 5(a), inset]. Therefore, it can be concluded from these calculations that the effect of the electrodiffusion is not significant. We then proceed to experiments, where we have measured the fluorescence and lifetime of the target biomarker molecules.

RESULTS AND DISCUSSION

To experimentally demonstrate how will the integration of DEP and plasmonic effects enhance the detection of biomarker molecules, we have used fluorescently labeled Avidin molecules (size: 68 kDa; ex: 500 nm, em: 515 nm; suspended in a buffer that has a conductivity of 0.03 S/m; Vector Laboratories Inc., Burlingame, CA) as the molecules of interest. Published literature reports have used similar molecules such as Bovine serum albumin (BSA) and IgG molecules to show their proof of concepts (Fu *et al.*, 2010 and Barik *et al.*, 2014). Published reports that utilize only plasmonic effects have reported detecting about 1 μM (Fu *et al.*, 2010). To demonstrate the quantification of low concentrations of Avidin molecules, we have used $\sim$1 pM Avidin molecules in our experiments. To find the optimum frequency of the electric field (positive DEP force) that can quickly bring molecules and place in hotspots, we varied the frequency from 50 kHz to 500 kHz and measured the number of Avidin molecules collected

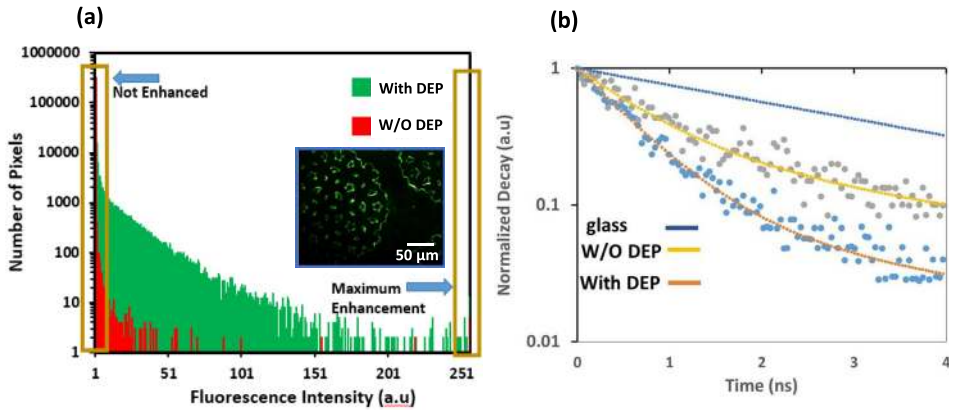

FIG. 5. The comparison and contrast of the effects of DEP in quantifying molecules using surface plasmonic effects. (a) Comparison of the fluorescence measured from a sample with and without DEP. Note that sample with DEP concentrates the Avidin molecules near the electrode edges and increases the fluorescence. Similarly, sample that has no DEP randomly scatters the molecules. The inset shows the picture of the sample with DEP used to generate the above plot. Further, we indicate the pixels where there are no plasmonic effects as well as there are significant plasmonic effects. (b) Fluorescence decay curves for the TRITC labeled biotin molecules in glass coverslip, on electrodes with DEP and on electrodes without DEP. These decay curves were used to calculate the lifetimes of the molecules in each case.

near the electrodes. Briefly, for each frequency, we recorded a fluorescence picture of the electrodes with molecules and measured the fluorescence intensity at the periphery of electrodes. We then choose the frequency that generated the highest fluorescence (120 kHz). We used this frequency for the experiments involving Avidin molecules. In experiments, briefly, we pipetted 1 pM Avidin molecules onto PIDEs and electric field (10 Vpp with 120 kHz) was applied to the terminals A and B [Fig. 1(a)] to concentrate Avidin molecules on the hotspots. The electric field was kept on (active) for 2–3 min to positive DEP to place molecules in the hotspots. We then turned off the electric field and imaged the PIDEs using a low-power fluorescent microscope and recorded the fluorescence image [inset of Fig. 5(a)]. We have turned off the electric field to avoid any interference from the electric field during fluorescence microscopy. After turning off the electric field, we have recorded a fluorescence image instantly (<5 s). Since the DEP off time is very short, Avidin molecules did not move away from hotspots during the fluorescence measurements. Further, we have also noticed that the Avidin molecules that are extracted by positive DEP near the electrodes do not scatter out immediately after turning off the DEP force. To compare the effects of DEP concentrating biomarker molecules in hotspots, we have performed another experiment using another PIDE array without applying DEP. Finally, using a custom made software program, we have extracted the fluorescence intensity of each pixel of each image and plotted for comparison. Figure 5(a) illustrates the fluorescence intensity vs. the number of pixels for the two experiments discussed above. By simple comparison, we can conclude that there is a large-number of bright pixels in the sample with DEP (plotted in green) when compared with the same sample that had no DEP (plotted in red). Therefore, we have assumed that DEP effectively concentrated the biomarkers on the hotspots and biomarker molecules in the hotspots are subjected to plasmonic effects and produce high fluorescence signal. Further, in Fig. 5(a), we indicate the pixels, where there are no plasmonic effects as well as there are significant plasmonic effects. If DEP places molecules in the hotspots, those molecules must have a significant reduction in the fluorescence lifetime. To experimentally show this, we used fluorescence lifetime spectroscopy.

The purpose of measuring the lifetime is based on the hypothesis that the biomarkers in the hotspots will have a significantly shorter fluorescence lifetime than the biomarkers that are not under the influence of the plasmonic effect. There are a number of methods available for measuring fluorescence lifetimes (Brismar *et al.*, 1995). Time-correlated single photon counting (TCSPC) is commonly used in many applications in which exponential decay of fluorescence light intensity is measured and used to calculate the lifetimes (Brismar *et al.*, 1995). The detailed procedure for calculating the lifetime of a sample is published elsewhere (Brismar *et al.*, 1995). To measure the lifetimes of molecules that are placed in the hotspots, we have used 150 nM, tetramethylrhodamine (TRITC) labeled streptavidin molecules (ProteinMods, Madison, WI). The selection of TRIC labeled streptavidin molecules is based on the optical capabilities that we had in the lab. We measured the fluorescence lifetime of streptavidin TRITC using the TCSPC system that we designed and assembled in the lab. The detailed illustration of the experimental set-up is included in the supplementary material figures. Briefly, our TCSPC system consists of the following parts: A Teem Photonics Microchip NanoPulse NP-10820–100 Nd:YAG laser at 1064 nm with a pulse duration of 590 ps, an energy per pulse of 10 μJ, and a pulse-repetition rate of 6.9 kHz, a Potassium dihydrogen phosphate (KDP) nonlinear crystal to convert the laser output to 532 nm through second harmonic generation, a Zeiss Axiovert 40C microscope with an 100× objective, an Ocean Optics 532 nm notch filter, a Fisher Scientific monochromator tuned at 572 nm with an full-width at half maximum bandwidth of 8 nm, a Hamamatsu photomultiplier tube R7207-01 powered by an 800 V source, a Hamamatsu photon counting unit C6465, an Agilent infinium 54853A DSO oscilloscope with 20 Gsa/s, and a photodiode Electro-Optics ET-2040.

In experiments, we have suspended the TRITC labeled streptavidin molecules in 0.01× phosphate buffered saline (PBS) buffer and pipetted about 100 μl of streptavidin over the electrodes and applied an external electric field (using electric potential of 10 Vpp and 400 kHz) and placed the molecules on the hotspots. As before, we applied the electric field and left it on for 2–3 min for fluorescent molecules to experience DEP and move to hotspots. The selection

of frequency (400 kHz) and voltage (10 Vpp) was chosen to generate the highest DEP force on TRITC molecules. To find the frequency and voltage, we started with 120 kHz and 1 Vpp and gradually increase the frequency and voltage and observed the motion of TRITC molecules. At 400 kHz and 10 Vpp, these molecules experience the largest positive DEP force. We then turned off the DEP and measured the photons that are emitted from the sample with time. These values are represented as points in Fig. 5(b). Finally, using the photon vs. time, we calculated the fluorescence decay of TRITC labeled streptavidin with time. Finally, we used the least squares algorithm to calculate the amplitude and the decay coefficient of the two exponential components of the fluorescence decay of TRITC that best fit the data obtained with our TCSPC system in samples that have the metal-glass interface without DEP and the metal-glass interface with DEP. The only difference between these two samples was the DEP, and all other experimental parameters remained unchanged. The goodness of each fit was calculated using R-square, and the values were 0.976 and 0.979 for the sample with DEP and without DEP, respectively. The equations with the respective coefficients in the metal-glass interface are

$$I_{wDEP}(t) = 0.92e^{-1.67t} + 0.08e^{-0.25t}, \quad I_{w/oDEP}(t) = 0.75e^{-1.38t} + 0.25e^{-0.24t}. \tag{6}$$

The equations ($I_{w/oDEP}$ and I_{wDEP} denote the fluorescence intensity without and with DEP, respectively) in (6) are plotted in Fig. 5(b). The second exponential component in both equations has a decay coefficient (0.25 and 0.24) whose inverse is consistent with the reported fluorescence lifetime of conjugated TRITC (Brismar *et al.*, 1995). The first exponential component in both equations had decay coefficients (1.67 and 1.38) whose inverse is close to the duration of the pulses from the Q-switched laser. Previous studies indicated the fast exponential decay, which is due to the surface plasmonic effect (Brismar *et al.*, 1995). The lifetime of the sample that underwent positive DEP is $\left(\frac{1}{1.67} = 0.6\right)$ 0.6 ns, and the lifetime of the sample without positive DEP is $\left(\frac{1}{1.38} = 0.72\right)$ 0.72 ns. This reduction in lifetime is due to the DEP concentrating streptavidin molecules in the hotspots. Furthermore, our laser that we used in the lifetime studies was a pulsed laser with a pulse duration of 0.56 ns of full-width at half-maximum. Therefore, we will not be able to record the lifetimes that are smaller than 0.56 ns. The purpose of the lifetime experiments was to demonstrate that the sample that underwent positive DEP would have reduction in lifetime when compared with the sample that did not undergo DEP.

Finally, we have varied the molarity of Avidin molecules from 1.5 μM to 150 fM and recorded an image for each molarity. We then plotted the variation of fluorescence intensity versus the number of pixels. We have included the plot in supplementary material, Fig. 1(a). We then assumed that fluorescence intensities that are above 80 are significant and above the white noise level. According to this criterion, our integrated dielectrophoretic and plasmonics based technique is capable of detecting about 1.5 pM of Avidin molecules.

To compare the results and find the improvement in the detection, we have used the standard fluorescence technique and repeated the experiments. Briefly, we have pipetted about 100 μl of Avidin molecules (we varied molarities from 1.5 μM to 150 fM) and recorded a fluorescence image of the sample for each molarity. We then plotted the variation of fluorescence intensity versus the number of pixels for each molarity. The results are included in supplementary material, Fig. 1(b). We then assumed that fluorescence intensity that is above 80 is the valid intensity that is above the white noise level. According to our assumption, 1.5 μM is the smallest molarity that can be measured using the standard fluorescence. Therefore, by simple comparison (1.5 μM/1.5 pM = 1 000 000-fold), our integrated dielectrophoretic and plasmonics based technique enhances the detection of Avidin molecules by about 10^6-fold.

CONCLUSIONS

In summary, we have demonstrated the successful integration of our PIDEs with plasmonic hotspots for the detection of biomarker molecules. We have then experimentally showed that the positive DEP, indeed, efficiently brings biomarker molecules and places them in plasmonic hotspots. Finally, we experimentally measured a reduction in the fluorescence lifetime of the

molecules that are placed in the electrodes. The observed reduction in the lifetime of molecules is a direct result of the molecular interaction with enhanced electric fields in the hotspots and/or surface plasmon polaritons (SPPs). However, SPPs decay with the square of the electric field, and therefore, SPP effects will limit the smaller quantification of molecules that are near the electrode-glass interface. In contrast, we believe that molecular interactions with enhanced electric fields in hotspots do not depend on the proximity to the electrodes, and therefore, it will provide significant contribution to the measured reduction of fluorescence lifetime. These effects combinedly contributed to the observed 10^6-fold improvement of the current detection limit. Further, in this work, we did not decouple these two effects to find out the contribution of each phenomenon. The main purpose is to demonstrate the employment of DEP in placing molecules in strategic locations so that they will be subjected to plasmonic effects (SPPs or interacting with high electric fields in the hotspots). Finally, with few more modifications, this technology can be translated into equipment for detecting and quantifying disease related molecules in real biological samples at point-of-care settings.

SUPPLEMENTARY MATERIAL

See supplementary material for the following: Fig. 1, we have included the histograms of various molarities of Avidin molecules measured using our technique and standard fluorescence technique. In Fig. 2, we have included a schematic diagram of the experimental set-up used for lifetime measurements.

ACKNOWLEDGMENTS

We would like to thank Jeffery Erickson, Darrin Laudenbach, and Vidura Jayasooriya in the Electrical and Computer Engineering Department at the North Dakota State University (NDSU) for their help in experiments. We also thank the staff of the Center for Nanoscience and Engineering at the North Dakota State University for their help in fabricating PIDEs. Finally, we extend a special thanks to Dr. Paul Kelter in the office of teaching and learning at NDSU for proofreading the manuscript. D.N. acknowledges the financial support from the NDSU development foundation.

Barik, A., *et al*., "Dielectrophoresis-enhanced plasmonic sensing with gold nanohole arrays," Nano Lett. **14**(4), 2006–2012 (2014).

Basuray, S. and Chang, H. C., "Induced dipoles and dielectrophoresis of nanocolloids in electrolytes," Phys. Rev. E **75**(6), 060501(R) (2007).

Brismar, H., Trepte, O., and Ulfhake, B., "Spectra and fluorescence lifetimes of lissamine rhodamine, tetramethylrhodamine isothiocyanate, texas red, and cyanine 3.18 fluorophores: Influences of some environmental factors recorded with a confocal laser scanning microscope," J. Histochem. Cytochem. **43**(7), 699–707 (1995).

Čemažar, J., Douglas, T. A., Schmelz, E. M., and Davalos, R. V., "Enhanced contactless dielectrophoresis enrichment and isolation platform via cell-scale microstructures," Biomicrofluidics **10**(1), 014109 (2016).

Chaurey, V., Rohani, A., Su, Y. H., Liao, K. T., Chou, C. F., and Swami, N. S., "Scaling down constriction-based (electrodeless) dielectrophoresis devices for trapping nanoscale bioparticles in physiological media of high-conductivity," Electrophoresis **34**(7), 1097–1104 (2013).

Cheng, I. F., Senapati, S., Cheng, X., Basuray, S., Chang, H. C., and Chang, H. C., "A rapid field-use assay for mismatch number and location of hybridized DNAs," Lab Chip **10**(7), 828–831 (2010).

Clarke, R. W., White, S. S., Zhou, D., Ying, L., and Klenerman, D., "Trapping of proteins under physiological conditions in a nanopipette," Angew. Chem. Int. Ed. **44**(24), 3747–3750 (2005).

Cuervo, A., Dans, P. D., Carrascosa, J. L., Orozco, M., Gomila, G., and Fumagalli, L., "Direct measurement of the dielectric polarization properties of DNA," Proc. Natl. Acad. Sci. **111**(35), E3624–E3630 (2014).

Dutta Choudhury, S., Badugu, R., Ray, K., and Lakowicz, J. R., "Silver–gold nanocomposite substrates for metal-enhanced fluorescence: Ensemble and single-molecule spectroscopic studies," J. Phys. Chem. C. **116**(8), 5042–5048 (2012).

Epstein, J. R. and Walt, D. R., "Fluorescence-based fibre optic arrays: a universal platform for sensing," Chem. Soc. Rev. **32**(4), 203–214 (2003).

Ermolina, I. and Morgan, H., "The electrokinetic properties of latex particles: Comparison of electrophoresis and dielectrophoresis," J. Colloid Interface Sci. **285**(1), 419–428 (2005).

Fu, C. C., Ossato, G., Long, M., Digman, M. A., Gopinathan, A., Lee, L. P., Gratton, E., and Khine, M., "Bimetallic nanopetals for thousand-fold fluorescence enhancements," Appl. Phys. Lett. **97**(20), 203101 (2010).

Geddes, C. D. and Lakowicz, J. R., "Editorial: Metal-enhanced fluorescence," J. Fluoresc. **12**(2), 121–129 (2002).

Gupta, V., Jafferji, I., Garza, M., Melnikova, V. O., Hasegawa, D. K., Pethig, R., and Davis, D. W., "ApoStream^{TM}, a new dielectrophoretic device for antibody independent isolation and recovery of viable cancer cells from blood," Biomicrofluidics **6**(2), 024133 (2012).

Hughes, M. P., Morgan, H., and Flynn, M. F., "The dielectrophoretic behavior of submicron latex spheres: Influence of surface conductance," J. Colloid Interface Sci. **220**(2), 454–457 (1999).
Iandolo, B., Antosiewicz, T. J., Hellman, A., and Zorić, I., "On the mechanism for nanoplasmonic enhancement of photon to electron conversion in nanoparticle sensitized hematite films," Phys. Chem. Chem. Phys. **15**(14), 4947–4954 (2013).
Jolley, M. E., Wang, C. H. J., Ekenberg, S. J., Zuelke, M. S., and Kelso, D. M., "Particle concentration fluorescence immunoassay (PCFIA): A new, rapid immunoassay technique with high sensitivity," J. Immunol. Methods **67**(1), 21–35 (1984).
Kim, D., Daniel, W. L., and Mirkin, C. A., "Microarray-based multiplexed scanometric immunoassay for protein cancer markers using gold nanoparticle probes," Anal. Chem. **81**(21), 9183–9187 (2009).
Kim, S. K., Hesketh, P. J., Li, C., Thomas, J. H., Halsall, H. B., and Heineman, W. R., "Fabrication of comb interdigitated electrodes array (IDA) for a microbead-based electrochemical assay system," Biosens. Bioelectron. **20**(4), 887–894 (2004).
Lakowicz, J. R., "Radiative decay engineering: Biophysical and biomedical applications," Anal. Biochem. **298**(1), 1–24 (2001).
Li, H. and Bashir, R., "Dielectrophoretic separation and manipulation of live and heat-treated cells of Listeria on microfabricated devices with interdigitated electrodes," Sens. Actuators, B **86**(2), 215–221 (2002).
Liao, K. T., Tsegaye, M., Chaurey, V., Chou, C. F., and Swami, N. S., "Nano-constriction device for rapid protein preconcentration in physiological media through a balance of electrokinetic forces," Electrophoresis **33**(13), 1958–1966 (2012).
Lisi, P. J., Huang, C. W., Huffman, R. A., and Teipel, J. W., "A fluorescence immunoassay for soluble antigens employing flow cytometric detection," Clin. Chim. Acta **120**(2), 171–179 (1982).
Lu, G., *et al*., "Plasmonic-enhanced molecular fluorescence within isolated bowtie nano-apertures," ACS Nano **6**(2), 1438–1448 (2012).
Lu, Y., Liu, T., Lamanda, A. C., Sin, M. L., Gau, V., Liao, J. C., and Wong, P. K., "AC electrokinetics of physiological fluids for biomedical applications," J. Lab. Autom. **20**(6), 611–620 (2015).
Maier, S. A. and Atwater, H. A., "Plasmonics: Localization and guiding of electromagnetic energy in metal/dielectric structures," J. Appl. Phys. **98**(1), 011101 (2005).
Mendes, P. M., Jacke, S., Critchley, K., Plaza, J., Chen, Y., Nikitin, K., Palmer, R. E., Preece, J. A., Evans, S. D., and Fitzmaurice, D., "Gold nanoparticle patterning of silicon wafers using chemical e-beam lithography," Langmuir **20**(9), 3766–3768 (2004).
Mulvihill, M. J., Ling, X. Y., Henzie, J., and Yang, P., "Anisotropic etching of silver nanoparticles for plasmonic structures capable of single-particle SERS," J. Am. Chem. Soc. **132**(1), 268–274 (2009).
Nakano, A. and Ros, A., "Protein dielectrophoresis: advances, challenges, and applications," Electrophoresis **34**(7), 1085–1096 (2013).
Nakano, A., Luo, J., and Ros, A., "Temporal and spatial temperature measurement in insulator-based dielectrophoretic devices," Anal. Chem. **86**(13), 6516–6524 (2014).
Nawarathna, D., Norouzi, N., McLane, J., Sharma, H., Sharac, N., Grant, T., Chen, A., Strayer, S., Ragan, R., and Khine, M., "Shrink-induced sorting using integrated nanoscale magnetic traps," Appl. Phys. Lett. **102**(6), 063504 (2013).
Nawarathna, D., Turan, T., and Wickramasinghe, H. K., "Selective probing of mRNA expression levels within a living cell," Appl. Phys. Lett. **95**(8), 083117 (2009).
Patterson, G. H., Knobel, S. M., Sharif, W. D., Kain, S. R., and Piston, D. W., "Use of the green fluorescent protein and its mutants in quantitative fluorescence microscopy," Biophys. J. **73**(5), 2782 (1997).
Pethig, R., "Review article—dielectrophoresis: Status of the theory, technology, and applications," Biomicrofluidics **4**(2), 022811 (2010).
Pommer, M. S., Zhang, Y., Keerthi, N., Chen, D., Thomson, J. A., Meinhart, C. D., and Soh, H. T., "Dielectrophoretic separation of platelets from diluted whole blood in microfluidic channels," Electrophoresis **29**(6), 1213–1218 (2008).
Rusling, J. F., *et al*., "Measurement of biomarker proteins for point-of-care early detection and monitoring of cancer," Analyst **135**(10), 2496–2511 (2010).
Sanghavi, B. J., Varhue, W., Rohani, A., Liao, K. T., Bazydlo, L. A., Chou, C. F., and Swami, N. S., "Ultrafast immunoassays by coupling dielectrophoretic biomarker enrichment in nanoslit channel with electrochemical detection on graphene," Lab Chip **15**(24), 4563–4570 (2015).
White, I. M., Yazdi, S. H., and Wei, W. Y., "Optofluidic SERS: Synergizing photonics and microfluidics for chemical and biological analysis," Microfluid. Nanofluid. **13**(2), 205–216 (2012).
Wolcott, M. J., "Advances in nucleic acid-based detection methods," Clin. Microbiol. Rev. **5**(4), 370–386 (1992).
Zheng, L., Brody, J. P., and Burke, P. J., "Electronic manipulation of DNA, proteins, and nanoparticles for potential circuit assembly," Biosens. Bioelectron. **20**(3), 606–619 (2004).
Zou, Z., Kai, J., Rust, M. J., Han, J., and Ahn, C. H., "Functionalized nano interdigitated electrodes arrays on polymer with integrated microfluidics for direct bio-affinity sensing using impedimetric measurement," Sens. Actuators, A **136**(2), 518–526 (2007).